

CHEMISTRY

A **European** Journal

Supporting Information

© Copyright Wiley-VCH Verlag GmbH & Co. KGaA, 69451 Weinheim, 2014

Inherently Chiral Macrocyclic Oligothiophenes: Easily Accessible Electrosensitive Cavities with Outstanding Enantioselection Performances

Francesco Sannicolò,^{*[a]} Patrizia R. Mussini,^[a] Tiziana Benincori,^[b] Roberto Cirilli,^[c] Sergio Abbate,^[d] Serena Arnaboldi,^[a] Simone Casolo,^[a] Ettore Castiglioni,^[d] Giovanna Longhi,^[d] Rocco Martinazzo,^[a] Monica Panigati,^[a] Marco Pappini,^[e] Elsa Quartapelle Procopio,^[a] and Simona Rizzo^[f]

chem_201404331_sm_miscellaneous_information.pdf

Supporting Information

SI 1 Synthesis of **2** and **3**

SI 2 HR LDI of the mixture from FeCl₃ oxidation of (±)-**1a**

SI 3 HR LDI Spectra analysis

SI 4 Synthesis and characterization of (±)-**1b**

SI 5 HR LDI of the products from FeCl₃ oxidation of (±)-**1b**

SI 6 HR LDI of dimers mixture electrodeposited on ITO

SI 7 Separation and enantiomeric purity check of **2** and **3** resulting from the FeCl₃ oxidation of enantiopure **1a**

SI 8 ¹H and ¹³C NMR spectra of enantiopure **2** and **3**

SI 9 Theoretical Calculations

SI 10 Photophysical characterization

SI 11 Electrochemistry

SI 12 CPL and ECD Measurements

SI 13 The concept

SI 1

Synthesis of **2** and **3**

A solution of (\pm)-**1a**¹ (100 mg, 0.17 mmol) in dry chloroform (50 mL) is added dropwise to a suspension of FeCl₃ (109 mg, 0.67 mmol) in dry chloroform (150 mL), under argon atmosphere, under vigorous stirring, at r.t., in 2 hours. The dark purple mixture is stirred overnight, then the volume of the solvent is reduced to 70 mL by evaporation under reduced pressure and the remaining solution poured into 150 mL of MeOH. The mixture becomes bright orange; it is filtered and the orange solid suspended in 30 mL of MeOH, then hydrazine (4 drops) is added. The mixture is filtered and the orange-red solid (84 mg) is extracted with THF using a Soxhlet apparatus, affording a soluble residue (49 mg) composed by cyclic oligomers of **1a** (see paragraph below).

The same methodology was applied to (\pm)-**1b** and to the enantiopure antipodes of **1a**.

SI 2

HR LDI of the mixture from FeCl₃ oxidation of (±)-1a

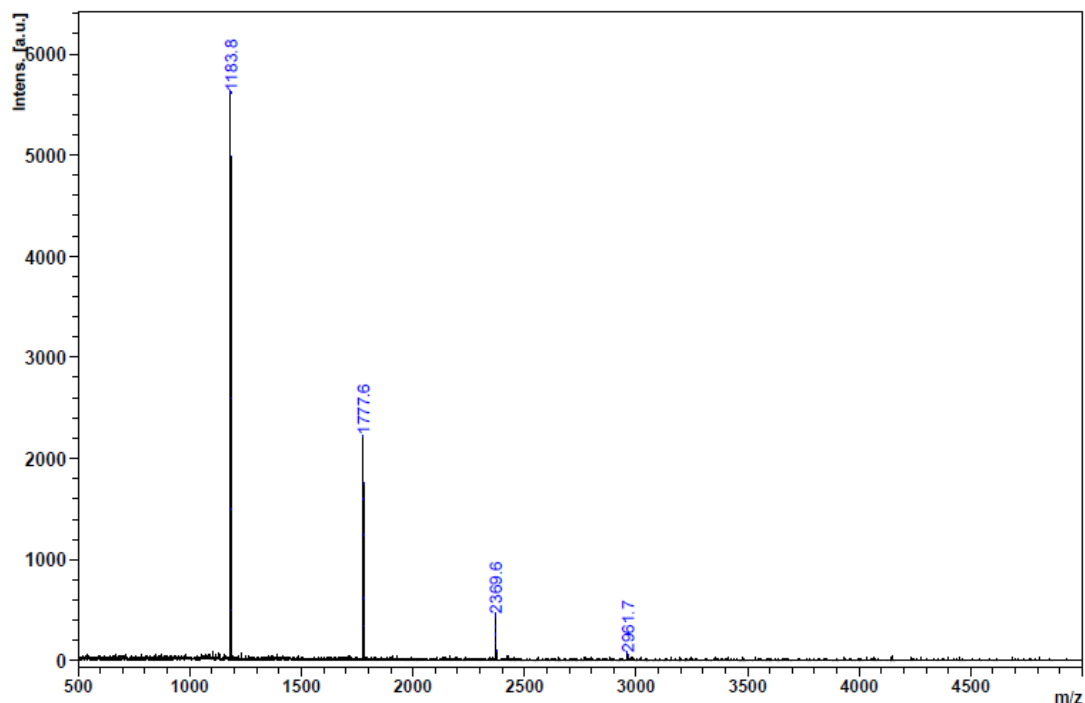


Figure S1. High Resolution LDI mass spectrometry of the residue obtained after Soxhlet extraction with THF in the range $m/z = 500-5000$.

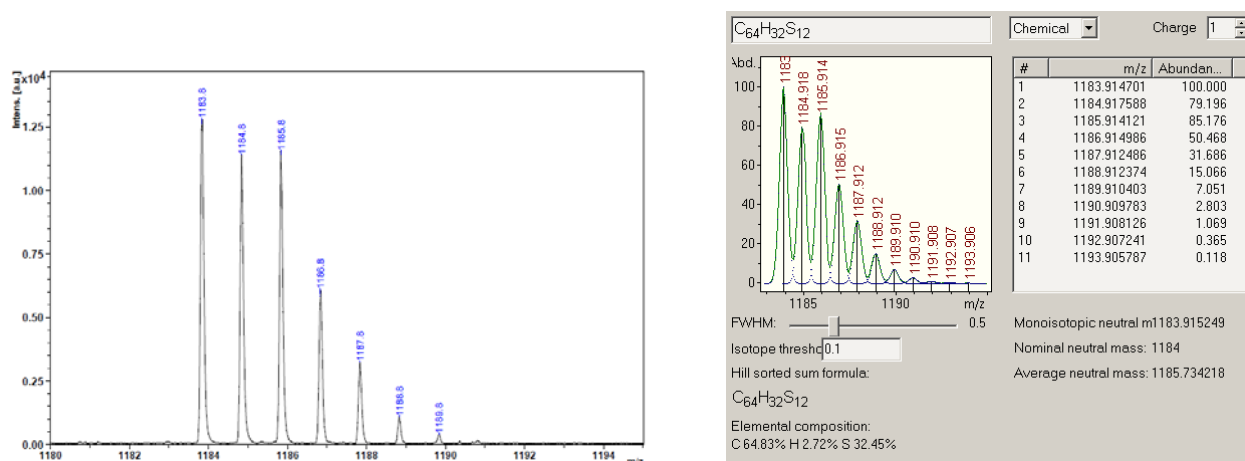


Figure S2. Experimental (left) and calculated ($C_{64}H_{32}S_{12}$, right) High Resolution LDI mass spectra of **2** in the range $m/z = 1180-1195$.

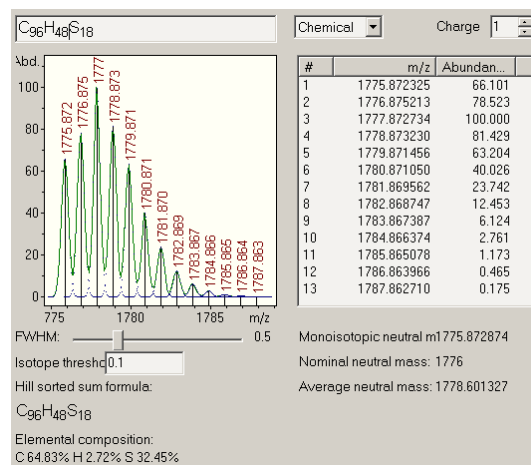
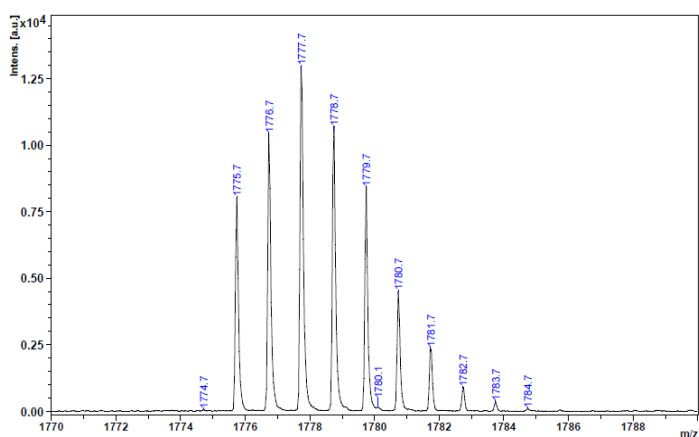


Figure S3. Experimental (left) and calculated ($C_{96}H_{48}S_{18}$, right) High Resolution LDI mass spectra of **3** in the range $m/z = 1770-1790$.

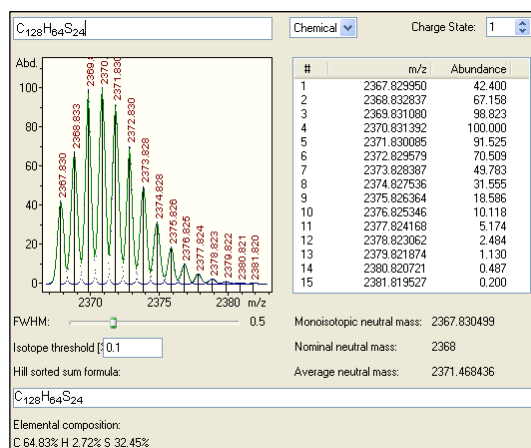
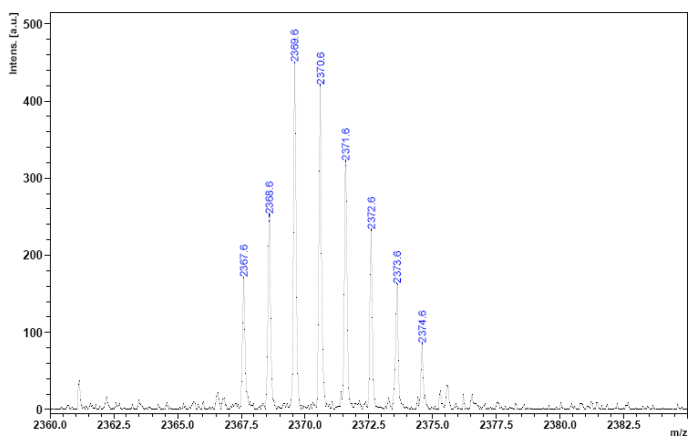


Figure S4. Experimental (left) and calculated ($C_{128}H_{64}S_{24}$, right) High Resolution LDI mass spectra of the stereoisomeric mixture of the cyclic tetramer of **1a** in the range $m/z = 2360-2390$.

SI 3

HR LDI Spectra analysis

High resolution LDI data were used to determine the relative abundance of cyclic *vs.* open-chain oligomers. To this end the mass spectra $I(x)$ (where x is the mass/charge ratio) were fitted to a (positive) superposition of basis signals S^i

$$I(x) = \sum_i \gamma_i^2 S^i(x - \eta) \quad \text{Eq.(1)}$$

one for each possible isomer i . Optimization was performed by minimizing the standard euclidean distance in the space of squared-integrable functions, defined for each oligomer in an appropriate spectral range (e.g. [1180-1198] m/z for the dimer and [1775-1980] m/z for the trimer). Quadrature of the integrals was performed over the fine mass grid available from our instrument.

The basis signals S^i were obtained by the isotopologue abundances (as computed from the relevant elemental isotope abundances) upon Lorentzian broadening the theoretical δ -peaked distributions, using a common broadening factor for each signal.

A shift term η was added to the functional form Eq.(1) to allow for a possible drift of the mass signal. It was optimized in the fitting procedure, along with the broadening factor above and the coefficients γ_i , and always turned out to be much smaller than 1 m/z unit.

SI 4

Synthesis and characterization of (\pm)-**1b**

A 1.6 M solution *n*-BuLi in *n*-hexane (0.31 mL, 0.50 mmol) is dropped into a solution of (\pm)-**1a** (100 mg, 0.17 mmol) and tetramethyl-ethylenediamine (0.078 mL, 0.97 mmol) in THF (6 mL) under stirring, under nitrogen atmosphere, at -78°C , in ten minutes. The mixture is left under stirring at -70°C for 20 minutes, then the cooling bath is removed and D_2O (99.9% deuterium, 0.5 mL) is cautiously added. The solvent is removed under reduced pressure and the organic material extracted with Et_2O . The organic layer is dried (MgSO_4) and evaporated to dryness to give (\pm)-**1b**, which is used without any further purification.

The ^1H NMR spectrum of (\pm)-**1b** (CDCl_3 , 300 MHz) shows the nearly complete disappearance of the doublet present in the spectrum of (\pm)-**1a** at 7.20 ppm (Figure S5).

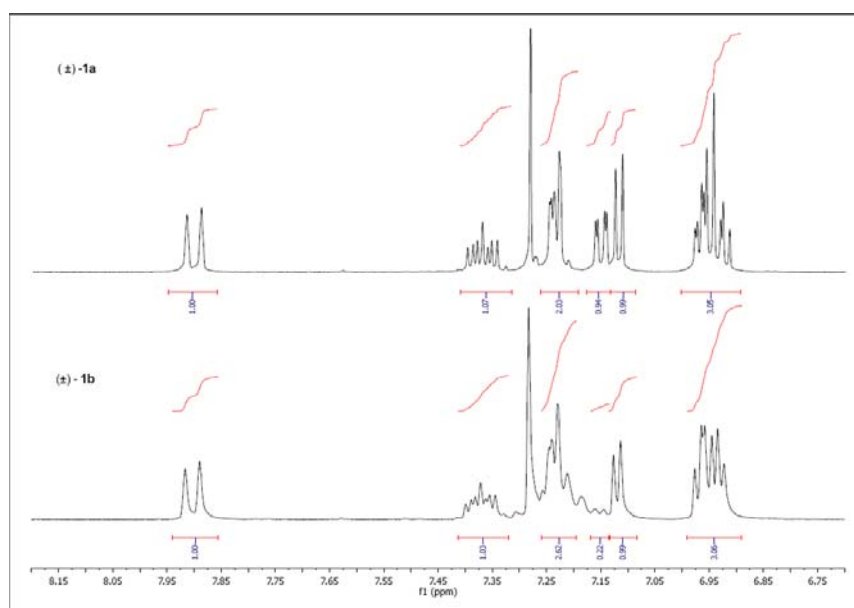


Figure S5. ^1H NMR spectrum of (\pm)-**1b** (CDCl_3 , 300 MHz).

The mass spectrum (HR-LDI) demonstrates that **1b** is a mixture of largely prevailing dideuterated (83.9%), monodeuterated (13.4%) and non deuterated (2.7%) compounds (Figure S6).

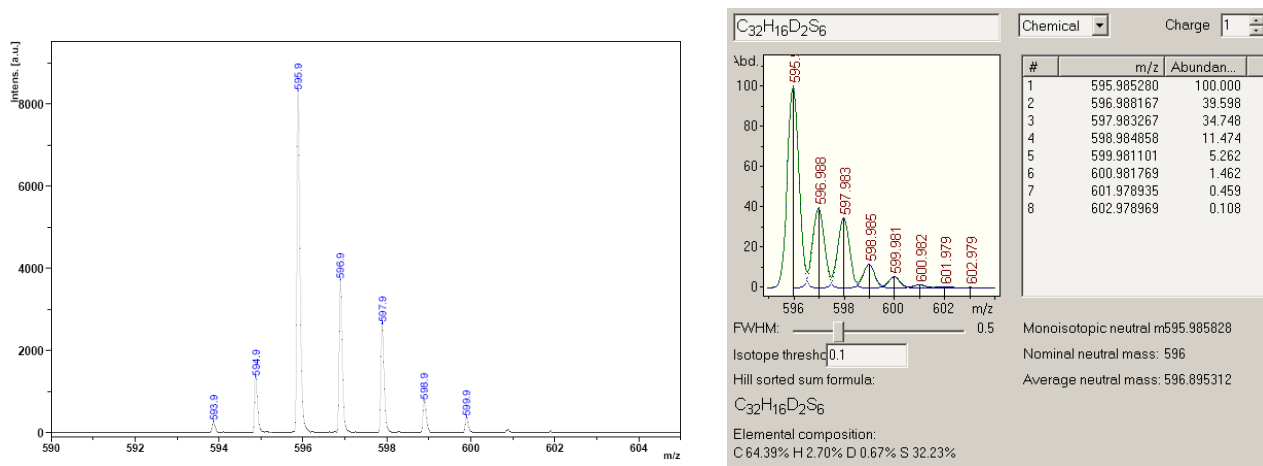


Figure S6. Experimental High Resolution LDI mass spectrum of deuterated **1b** (left, first row) and theoretical spectra of the dideuterated **1b**.

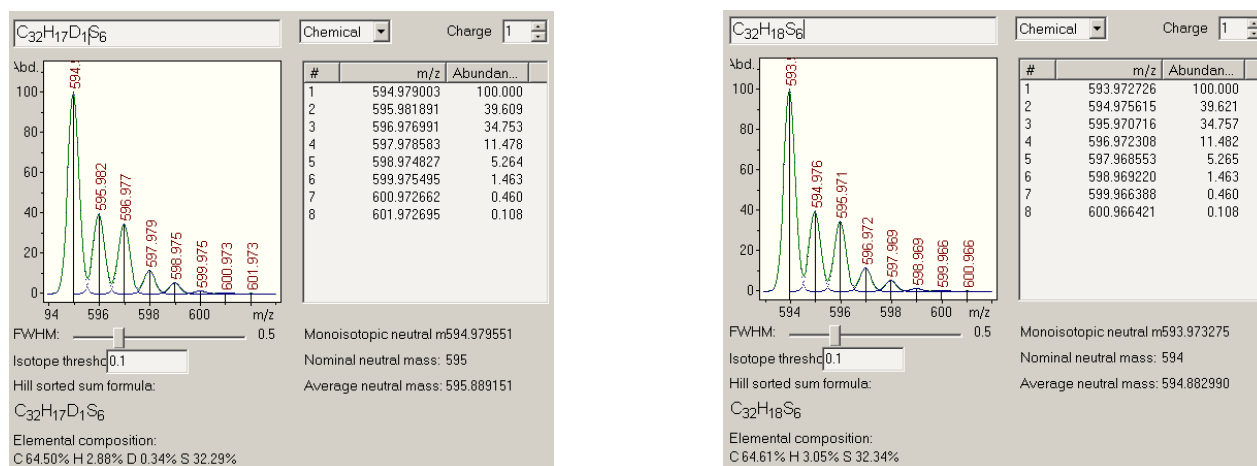


Figure S7. Theoretical High Resolution LDI mass spectra of the monodeuterated and non deuterated **1a**.

SI 5

HR LDI of the products from FeCl₃ oxidation of (±)-**1b**

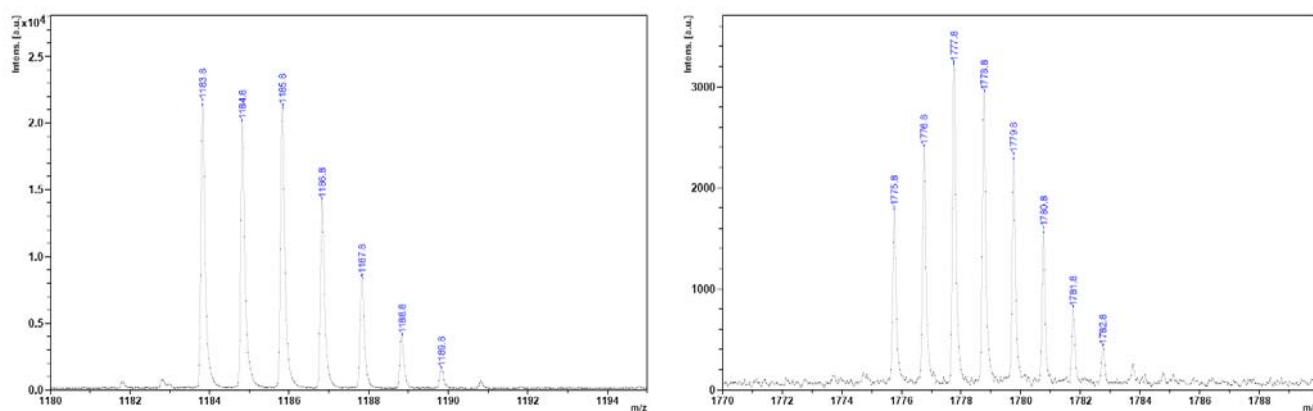


Figure S8. Experimental High Resolution LDI mass spectra of **2** (left) and **3** (right) resulting from the FeCl₃ oxidation of deuterated (±)-**1b**. Both the spectra correspond to non-deuterated compounds (see above **S2** and **S3**).

SI 6

HR LDI of the mixture of dimers electrodeposited on ITO

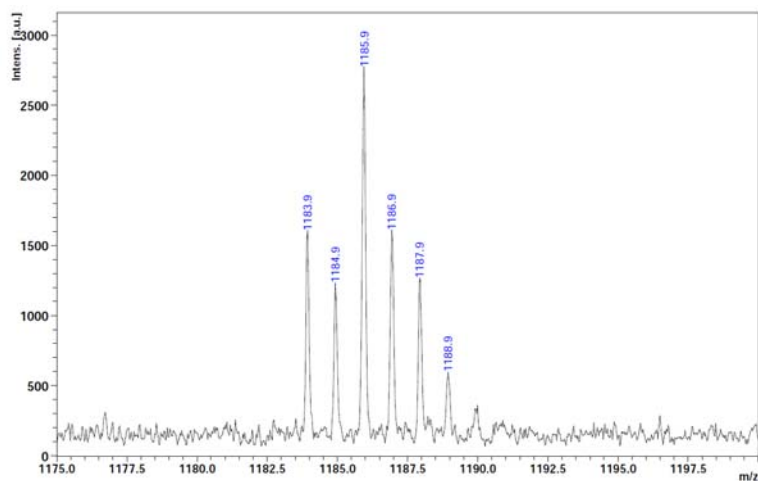


Figure S9. Experimental High Resolution LDI mass spectrum of the mixture of dimers resulting from the electrooxidation of (±)-**1a** on ITO electrode. The 51.9% corresponds to cyclic dimers **2** and the 48.1% to open-chain dimers.

SI 7

Separation and enantiomeric purity check of **2** and **3** resulting from the FeCl_3 oxidation of enantiopure **1a**

Applying the procedure described in paragraph **SI 1** to the enantiopure antipodes of **1a**, followed by accurate column chromatography (silica gel, eluent: hexane: CH_2Cl_2 -7:3) of the Soxhlet extract, enabled us to isolate the enantiopure dimer (S,S) -(-)-**2** and the (S,S,S) -(+)-**3** trimer from (S) -(+)-**1a** and, specularly, the (R,R) -(+)-**2** dimer and the (R,R,R) -(-)-**3** trimer from (R) -(-)-**1a**. The combined first fractions eluted, after evaporation of the solvent under reduced pressure, gave **2** as an orange solid (15 mg, 15% yields calculated on **1a**). Similarly, the second eluted series of fractions, after evaporation of the solvent under reduced pressure, gave **3** as an orange solid (8 mg, 8% yields calculated on **1a**).

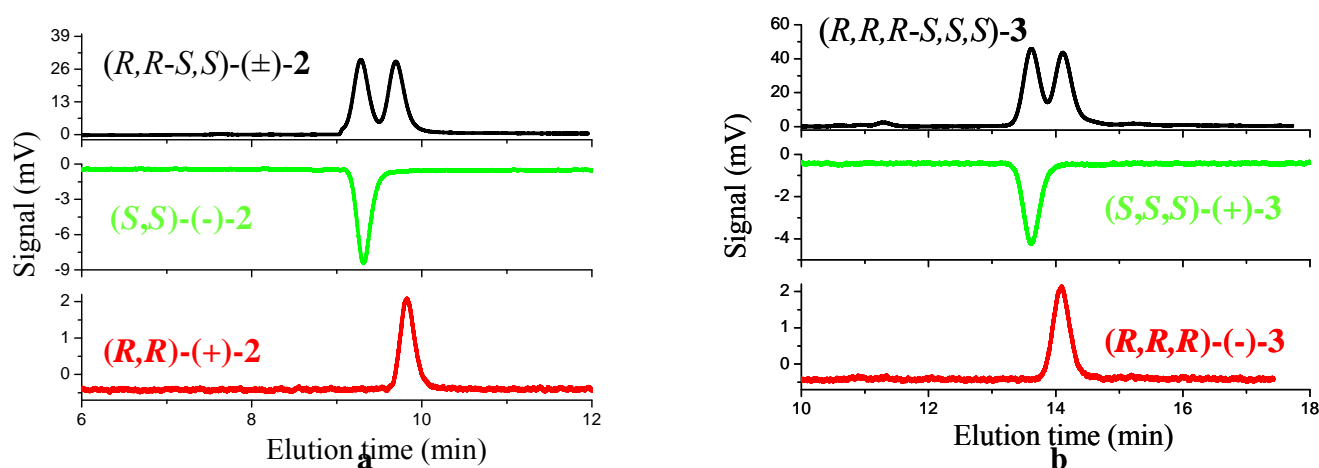
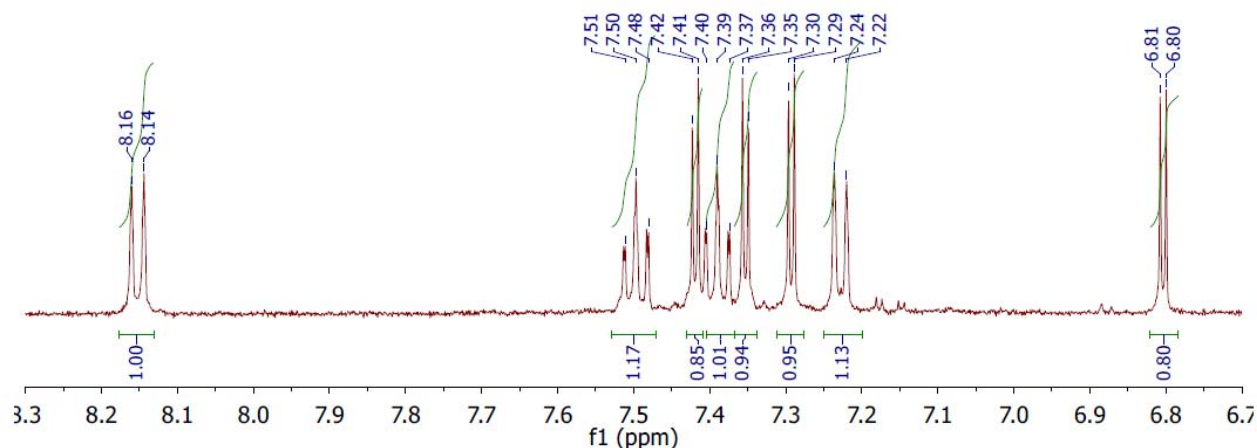


Figure S10. a. Analytical HPLC enantiomeric purity check on a chiral stationary phase of (S,S) -(-)-**2** (green) and (R,R) -(+)-**2** (red); racemate (black) prepared from pure enantiomers. CSP: Chiralpak IB-3 (250 mm x 4.6 mm I.D.) + Chiralpak IB-3 (100 mm x 4.6 mm I.D.); eluent: acetone:ethanol-100:60; flow rate: 1 mL/min; temperature: 5°C; detector: UV (black) and CD (green/red) at 410 nm. **b.** Enantiomeric purity check of (S,S,S) -(+)-**3** (green) and (R,R,R) -(-)-**3** (red); racemate (black) prepared from pure enantiomers. Conditions as reported for Figure S10a.

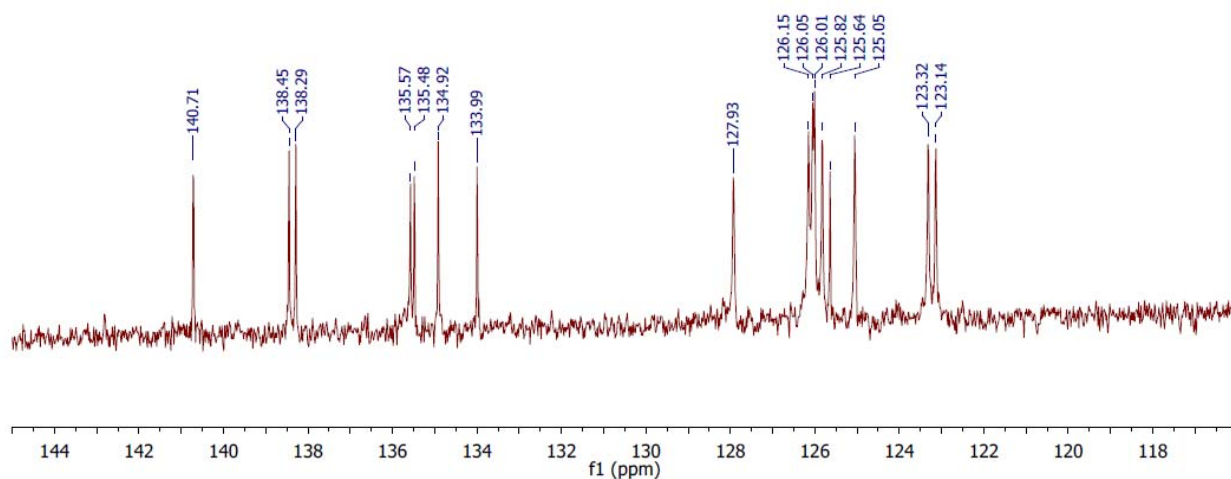
SI 8

^1H and ^{13}C NMR spectra of (*R,R*)-2/(*S,S*)-2 and of (*R,R,R*)-3/(*S,S,S*)-3

(*R,R*)- and (*S,S*)-2

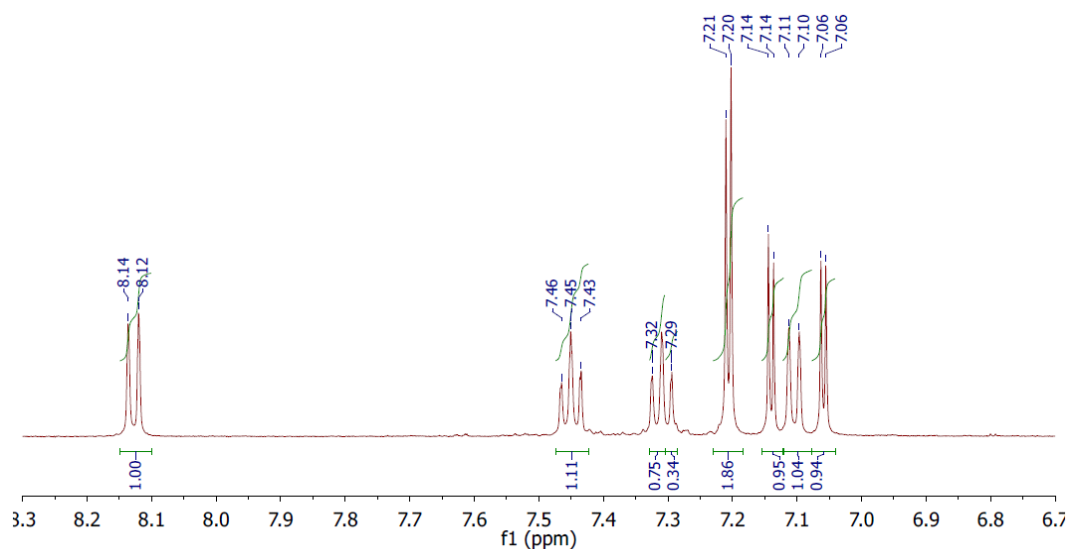


^1H NMR (500 MHz, CD_3SOCD_3 , 40 °C): δ = 8.15 (d, $^3J(\text{H,H})$ = 8.1 Hz, 4H), 7.50 (t, $^3J(\text{H,H})$ = 7.7 Hz, 4H), 7.42 (d, $^3J(\text{H,H})$ = 3.9 Hz, 4H), 7.39 (t, $^3J(\text{H,H})$ = 7. Hz, 4H), 7.35 (d, $^3J(\text{H,H})$ = 3.8 Hz, 4H), 7.29 (d, $^3J(\text{H,H})$ = 3.8 Hz, 4H), 7.23 (d, $^3J(\text{H,H})$ = 8.0 Hz, 4H), 6.80 (d, $^3J(\text{H,H})$ = 3.9 Hz, 4H).

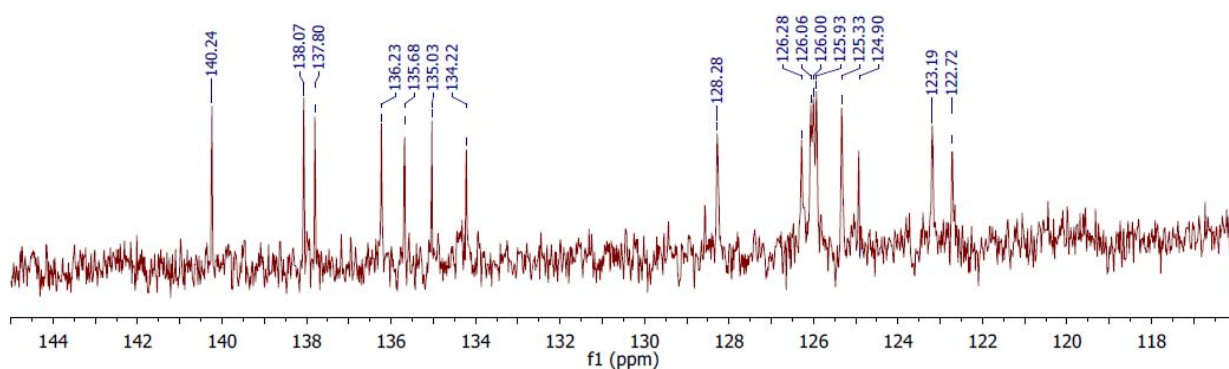


^{13}C NMR (9.4 T, CD_3SOCD_3 , 40 °C): δ = 140.71 (C), 138.45 (C), 138.29 (C), 135.57 (C), 135.48 (C), 134.92 (C), 133.99 (C), 127.93 (C), 126.15 (CH), 126.05 (CH), 126.01 (CH), 125.82 (CH), 125.64 (CH), 125.05 (CH), 123.32 (CH), 123.14 (CH).

Figure S11. ^1H NMR (above) and ^{13}C NMR spectra of (*R,R/S,S*)-2 (CD_3SOCD_3 , 40 °C). (*R,R,R*)-3 and (*S,S,S*)-3



^1H NMR (500 MHz, CD_3SOCD_3 , 40 °C): δ = 8.13 (d, $^3J(\text{H,H})$ = 8.0 Hz, 6H), 7.45 (t, $^3J(\text{H,H})$ = 7.6 Hz, 6H), 7.31 (t, $^3J(\text{H,H})$ = 7.6 Hz, 6H), 7.21 (d, $^3J(\text{H,H})$ = 4.0 Hz, 12H), 7.14 (d, $^3J(\text{H,H})$ = 4.0 Hz, 6H), 7.10 (d, $^3J(\text{H,H})$ = 8.0 Hz, 6H), 7.06 (d, $^3J(\text{H,H})$ = 3.8 Hz, 6H).



^{13}C NMR (9.4 T, CD_3SOCD_3 , 40 °C): δ = 140.24 (C), 138.07 (C), 137.80 (C), 136.23 (C), 135.68 (C), 135.03 (C), 134.22 (C), 128.28 (C), 126.28 (CH), 126.06 (CH), 126.00 (CH), 125.93 (CH), 125.33 (CH), 124.90 (CH), 123.19 (CH), 122.72 (CH).

Figure S12. ^1H NMR (above) and ^{13}C NMR spectra of (*R,R,R/S,S,S*)-**2** ($d_6\text{DMSO}$, 40 °C).

SI 9

Theoretical Calculations

Density Functional Theory calculations were performed within the generalized gradient approximation, employing the Perdew-Burke-Ernzerhof functional¹ to describe exchange-correlation effects.²

Calculations were performed in a periodic setting (using sufficiently large unit cells to accommodate each molecule and avoid interactions with their images) with the help of the efficient SIESTA *ab initio* code³ which uses a basis set of atomic orbitals⁴ and separable⁵ norm conserving pseudopotentials⁶ with partial core corrections.⁷ We used standard triple- ζ basis with polarization orbitals (TZP) and a large energy cutoff (1200 Ry) for the real space integration grid. Electronic convergence was enforced with a stringent energy criterion (10^{-5} eV) and geometry relaxation was performed until the forces acting on each atom were smaller than 0.005 eV/Å.

We checked *a posteriori* the optimized geometries by considering distortions along the soft modes, since geometry optimization is known to be critical in their presence. In the cyclic dimer **2**, for instance, we found that the major axis of the elliptical cavity is one such mode, and that the energy changes by less of 10 kJ mol⁻¹ for a tensile/compressive strain of up \pm 2%.

In order to investigate the reaction energetics, calculations were performed for both the cyclic structures and their open relatives, using several starting geometries in the optimization runs to identify the most stable conformer.

SI 10

Photophysical characterization

Absorption spectra were measured with an Agilent 8543 spectrometer at room temperature.

Steady-state emission spectra were recorded on a HORIBA Jobin-Yvon Fluorolog 3 spectrometer equipped with a 450W Xenon arc lamp and a Hamamatsu R928P photomultiplier tube as detector. Emission and excitation spectra were corrected for source intensity (lamp and grating) and emission spectral response (detector and grating) by standard correction curves.

For fluid solution state samples, luminescence quantum yields (PLQY) were measured in optically dilute solution and compared to reference emitters by the method of Demas and Crosby.⁸ The fluorescein in NaOH 0.1 M solution at room temperature was used as reference ($\Phi = 0.95$).⁹ All the PLQYs values fallen in a $\pm 5\%$ range.

SI 11

Electrochemistry

Racemic or enantiopure substrate films were deposited by drop casting from solutions of racemic or enantiopure **2** and **3** in CH_2Cl_2 on the gold working electrode of screen printed electrode minicells (Dropsens[®]), also featuring a carbon counter electrode and a silver pseudoreference electrode.

The solid-state CV features of the film-coated electrodes were recorded in the ionic liquid 1-butyl-3-methylimidazolium hexafluorophosphate, (BMIM)PF₆, by cyclic voltammetry, CV, performing redox cycles at different scan rates, using an AutolabPGSTAT potentiostat of Eco-Chemie (Utrecht, The Netherlands), run by a PC with the GPES software of the same manufacturer.

On the enantiopure electrode surfaces enantio-recognition tests were performed in the same conditions, using 0.012 M solutions of 1-ferrocenylethylamine probes (*S*)-**4** and (*R*)-**4** (Aldrich) or their racemate in (BMIM)PF₆ working medium.

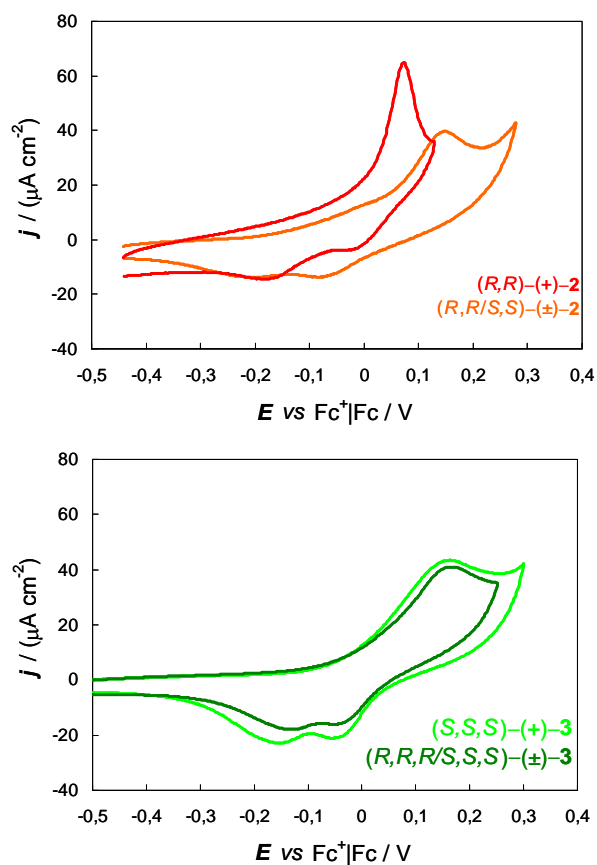


Figure S13. CV stability redox cycles of: *(R,R)*-(+)-**2** and (\pm) -**2**; **b.** *(S,S,S)*-(+)-**3** and (\pm) -**3**. Drop-casted films on screen printed electrodes (Au working electrode drop-casted with the same amount of material in weight, carbon counter electrode, Ag pseudo-reference electrode); (BMIM)PF₆ ionic liquid as the working medium; 0.05 V/s scan rate.

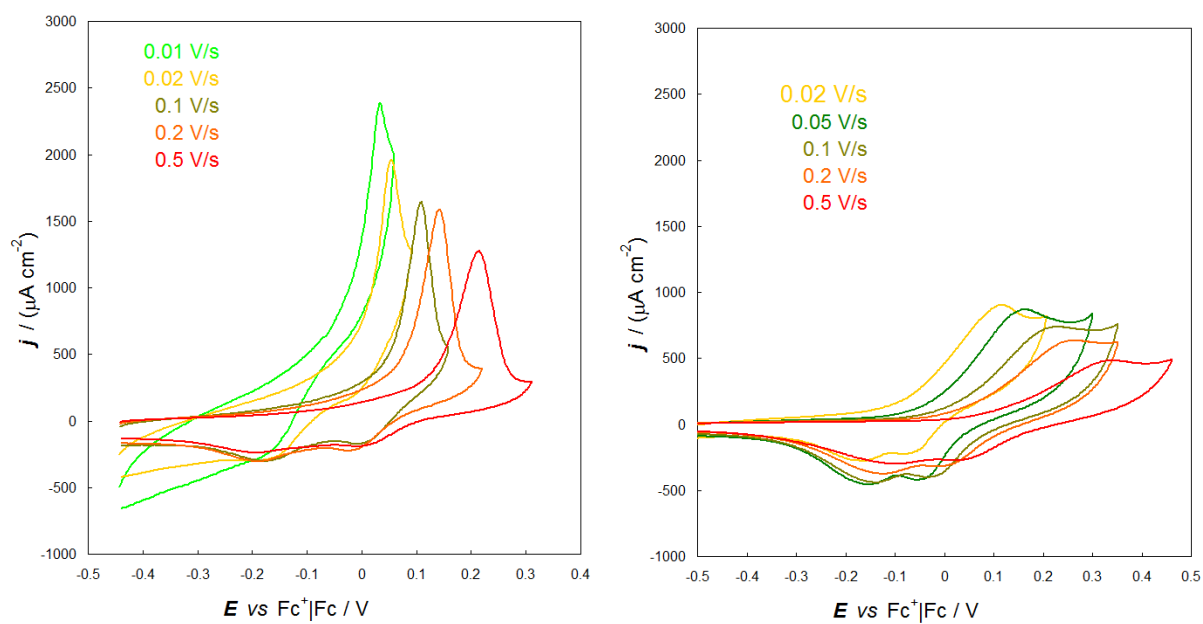


Figure S14. Scan rate effect on the electroactivity test of the films of drop-casted *(R,R)*-(+)-**2** and *(S,S,S)*-(+)-**3** on screen printed Au in (BMIM)PF₆.

SI 12

CPL and ECD Measurements

ECD measurements were conducted using a Jasco 815SE apparatus.

Fluorescence and circularly polarized luminescence spectra were recorded simultaneously using a homemade instrument, described in previous papers.^[10] The excitation radiation was brought to the cell from a Jasco FP8200 fluorimeter through an optical fiber containing water, a 90° scattering geometry was chosen, the incident radiation has been polarized parallel to the collection direction, 5 scans were taken for each enantiomer. Spectral response has been corrected using a reference lamp.

SI 13

The concept



Crop D_2 circle in a wheat field
at West Overton, near Lockeridge
Wiltshire
(Reported 9th August 2009)



Crop D_3 circle in a wheat field
at Barbury Castle, Wiltshire
(Reported 23rd July 1999)

Figure S15.

Photographs: courtesy of Mr. Steve Alexander - www.temporarytemples.co.uk.

References of the Supporting Information

- (1) F. Sannicolò, S. Rizzo, T. Benincori, W. Kutner, K. Noworyta, W. J. Sobczak, V. Bonometti, L. Falciola, P. R. Mussini, M. Pierini, *Electrochim. Acta* **2010**, *55*, 8352.
- (2) (a) J. P. Perdew, K. Burke, M. Ernzerhof, *Phys. Rev. Lett.* **1996**, *77*, 3865. (b) J. P. Perdew, K. Burke, M. Ernzerhof, *Phys. Rev. Lett.* **1997**, *78*, 1396.
- (3) G. A. Crosby, J. N. Demas, *J. Am. Chem. Soc.* **1970**, *92*, 7262.
- (4) O. F. Sankey, D. J. Niklewski, *Phys. Rev. B* **1989**, *40*, 3979.
- (5) L. Kleinman, D. M Bylander, *Phys. Rev. Lett.* **1982**, *48*,1425.
- (6) N. Troullier, J. L Martins, *Phys. Rev. B* **1991**, *43*,1993.
- (7) S. G. Louie, S. Froyen, M. L Cohen, *Phys. Rev. B* **1982**, *26*, 1738.
- (8) G. A. Crosby, J. N. Demas, *J. Am. Chem. Soc.* **1970**, *92*, 7262.
- (9) M. Takayanagi, T. Gejo, I. Hanazaki, *J. Phys. Chem.* **1994**, *98*, 12893.
- (10) (a) E. Castiglioni, S. Abbate, G. Longhi, *Appl. Spectrosc.* **2010**, *64*, 1416. (b) E.Castiglioni, S. Abbate, F. Lebon, G. Longhi, *Chirality* **2012**, *24*, 725.